JOURNAL OF EXPERIMENTAL AND THEORETICAL PHYSICS, 2024, Vol. 166, No. 3 (9), pp. 313–323

NUCLEI, PARTICLES, FIELDS, GRAVITY AND ASTROPHYSICS

FREQUENCY-TIME ANALYSIS OF RADON EMISSIONS CHANGES IN THE LNGS UNDERGROUND LABORATORY MEASURED BY THE LVD DETECTOR

© 2024 V. F. Yakushev *, N. Yu. Agafonova **, V. V. Ashikhmin, E. A. Dobrynina***, R. I. Enikeeva, N. A. Filimonovaa, I. R. Shakiryanova (on behalf of the LVD Collaboration)

Institute for Nuclear Research, Russian Academy of Sciences 117312, Moscow, Russia

* e-mail: yakushevvaleriy897@gmail.com
** e-mail: agafonova@inr.ru
*** e-mail: dobrynina02@mail.ru

Received February 13, 2024
Revised April 23, 2024
Accepted April 24, 2024

Abstract. A time-frequency analysis of time series of gamma-ray count rates measured by the LVD detector at the LNGS Laboratory, Gran Sasso, Italy is presented. The change in the gamma quanta counting rate is associated with radon emissions into the atmosphere of the underground hall of the Laboratory. Radioactive gas radon enters the room through microcracks and pore water from the ground. Radon variations are influenced by the gravitational effects of the rotation of the Sun and Earth, as well as ground movements from seismic events in the Italian region. Using the discrete Fourier transform, daily (solar and lunar), semi-diurnal, lunar-monthly, weekly and annual periods were found.

Keywords: *Radon, underground physics, Fourier analysis*

DOI: 10.31857/S004445102409e0491

1. INTRODUCTION

Radon ^{222}Rn is formed in rock as a result of fission and decay of uranium and thorium series elements [1] and enters the underground hall atmosphere through multiple microcracks in the rock or from water saturated with radon (radon is highly soluble in water) on its way through the rock mass to the underground hall.

The decrease in radon concentration occurs a) due to decay (radon half-life is 3.825 days), b) due to migration from the surrounding rock mass into the air. However, new gas generation appears from the uranium decay chain. Therefore, the average radon content in rock is always constant and is determined by the concentration of uranium (radium) in this mass. Radon migration in the rock mass and its release from the surface are determined by the macroscopic diffusion coefficient, which depends on many factors. The most important of these are porosity, permeability and fracturing. Since the number of microcracks increases during earth's crust deformations during earthquakes or as a result of gravitational tides from the Sun and Moon, radon emanation should also increase.

At the LVD setup which will be described in Section 2, it is possible to observe radon emissions associated with gravitational tides, anthropogenic activity (micro-tremors), and seismic activity in the region [2]. This research can become another tool for creating a comprehensive observation system and help geophysicists in predicting destructive earthquakes.

From the low-energy background of LVD, using the epoch folding method, annual variations in the gamma-ray counting rate from radon decay were obtained $\mathrm{d}N = (4 \pm 2)\%$, which are related to soil water saturation [3]. In recent works [4,5] at LVD, anthropogenic weekly and daily variations in

gamma-ray count rates were detected, and lunar-monthly variations were found using the epoch folding method [6].

The aim of this work is to conduct harmonic analysis using the discrete Fourier transform method of the continuous time series of gamma-ray counting rates to find the periods of harmonics, associated with gravitational tides from the Sun and Moon movements - these are solar-diurnal, lunar-diurnal, lunar periods, and annual period [7].

2. DESCRIPTION OF THE LVD SETUP AND EXPERIMENTAL DATA

The LVD detector [8] is located in the LNGS Laboratory [9] (Italy) at a depth of 3300 m.w.e. in a seismically active region under the Gran Sasso mountain massif. The three towers of the detector (T1, T2, T3) consist of 840 scintillation counters. Each counter with a size of 1.5 m^3 is filled with liquid scintillator based on white spirit (C_nH_{2n}, $n \approx 9.6$) and is viewed by three photomultiplier tubes (PMT). The total mass of the detector is 1 kt of iron and 1 kt of scintillator. The external counters of the facility, located next to the surrounding rock shield the internal counters (240 units) from the external radioactivity of the rock.

The LVD experiment is designed to detect neutrinos from stellar core collapses in our Galaxy. The detector background in the high-energy region consists of cosmic ray muons and products of their interaction in the detector material. In the low-energy region, the detector background consists of gamma rays from natural radioactivity of the rock and construction materials, as well as gamma rays from radioactive radon gas present in the underground hall atmosphere.

Gamma rays from the decay of radon and thoron daughter nuclei from uranium and thorium decay chains in the range from 0.5 to 3.5 MeV are registered by all detector counters during 10 s every 10 minutes.

Gamma radiation is mainly generated by nuclei ^{214}Bi, which through β-decay transform into ^{214}Po with a characteristic time of $\tau = 19.7$ min. The most probable decay chain:

$$^{222}\mathrm{Rn} \xrightarrow{\alpha} {}^{218}\mathrm{Po} \xrightarrow{\alpha} {}^{214}\mathrm{Pb} \xrightarrow{\beta^-} {}^{214}\mathrm{Bi} \xrightarrow{\beta^-} {}^{214}\mathrm{Po} \xrightarrow{\alpha} {}^{210}\mathrm{Pb}.$$

The number of gamma quanta from the thoron decay chain is almost an order of magnitude lower:

$$^{220}\mathrm{Rn} \xrightarrow{\alpha} {}^{216}\mathrm{Po} \xrightarrow{\alpha} {}^{212}\mathrm{Pb} \xrightarrow{\beta^-} {}^{212}\mathrm{Bi} \begin{cases} \xrightarrow{\beta^-} {}^{212}\mathrm{Po} \xrightarrow{\alpha} {}^{208}\mathrm{Pb}, \\ \xrightarrow{\alpha} {}^{208}\mathrm{Tl} \xrightarrow{\beta^-} {}^{208}\mathrm{Pb}. \end{cases}$$

The gamma-ray spectra and decay chains of ^{232}Th and ^{238}U are given in [10].

The number of counts due to radon for 70 internal counters of one tower is about 3150 per 10s. This sets the sensitivity of the method 5% at the level of 3σ, i.e., over a 10-second measurement interval, the setup will detect a 5-percent concentration deviation with reliability ~ 99.7 %. The registration method is described in detail in [11].

The detector has been operating since 1992. Time series of gamma-ray count rates are formed for the internal LVD counters of each tower, as the towers operate independently and differ slightly in their characteristics and location in the experimental hall [12].

The data represent the pulse count rate above the low energy threshold of ~ 0.5 MeV. Data is averaged across all LVD counters per one hour. The data have been cleaned. Thus, continuous time series were obtained for harmonic analysis $y_{T1}(t)$, $y_{T2}(t)$, $y_{T3}(t)$, T3 – radon counting rate of towers T1, T2 and T3 of the LVD detector in hertz, respectively.

Then the data are averaged only over the first and second towers, as the third tower differs somewhat structurally and in physical parameters (scintillator, PMT, detector design), i.e., $y(t) = (y_{T1}(t) + y_{T2}(t)) / 2$ for each hour. Total measurement time is 157800 h (18 years) from January 1, 2004. The statistical error in each bin of the input histogram y_n, $n = 1,..,$ 157800 can be determined by recalculating errors during data averaging. Systematic errors are difficult to estimate. There are many of them, and they change over time (temperature, supply voltage, changes in characteristics of scintillator, PMT, electronics over many years, etc.).

Therefore, it seems to be a good option to take the majority error in the form of standard deviation y_n over the entire measurement period T_{meas}:

$$s(y_n) = \sqrt{\frac{1}{157800}\sum_{n=1}^{157800}(\bar{y} - y_n)^2}. \quad (1)$$

This will automatically include all statistical and varying systematic errors. The result for errors: $\bar{y} = 59.18$ Hz, $s(y_n) = 9.82$ Hz. This majority error estimate is the same for all y_n. Now we have two time series y_n and $s(y_n)$. This is all that is needed for Fourier analysis.

3. FOURIER ANALYSIS

Discrete Fourier analysis was conducted using Bessel formulas to find the amplitudes of cosine and sine harmonics with zero phase, and then the result was reduced to a single cosine function (without sine) with non-zero phase (for simple graphical representation of results).

Along with calculating the harmonics amplitudes and their phases, error propagation was performed (based on $s(y_n)$). The error propagation formula is standard:

$$s(z_m(y_n)) = \sqrt{\sum_{n=1}^{157800}\left(\frac{\partial z}{\partial y_n}s(y_n)\right)^2},$$

where $z_m(y_n)$ is the amplitude of the function A_m of the harmonic with index m, depending on all values y_n of the input radon histogram, $s(y_n)$ is the error y_n.

There were 157800 (18 years) measurements (n = 1, … , 157800), so the number of harmonics at the output equals 157800 / 2 = 78900 (m = 1, … , 78900). The period of harmonic number $m = 1$ (the slowest): $T_1 = 157800$ h = 18 years (frequency $f_1 = 1 / T_1$).

The period of harmonic number 78900 (the fastest): $f_{78900} = 2$ h (frequency $f_{78900} = 1 / f_{78900}$). The relationship between harmonic number m and its period T_m: $T_m = 157800 / m$.

To later evaluate the significance of any harmonic based on its amplitude, the program also calculates the amplitude B_m of harmonics of equivalent power white noise (and error $s(B_m)$. In white noise, all harmonics have the same amplitude $B = B_m$.

Let A_m be the amplitude of the harmonic of radon data with index m ; $s(A_m)$ is the error A_m . The power of a harmonic is proportional to the square of its amplitude.

Then $B^2 \times 78900 = \sum_{m=1}^{78900} A_m^2$, consequently, the white noise amplitude

$$B = B_m = \sqrt{\frac{1}{78900}\sum_{n=1}^{78900} A_m^2} \text{ [Hz]}.$$

As a result, we get $B = 0.0495$ Hz, $s(B) = 6.66 \cdot 10^{-4}$ Hz is the standard error of value B. Let's calculate the significance of each harmonic:

$$\eta_m = \frac{A_m - B}{s(A_m - B)} = \frac{A_m - B}{\sqrt{(s(A_m))^2 + (s(B))^2}}. \quad (2)$$

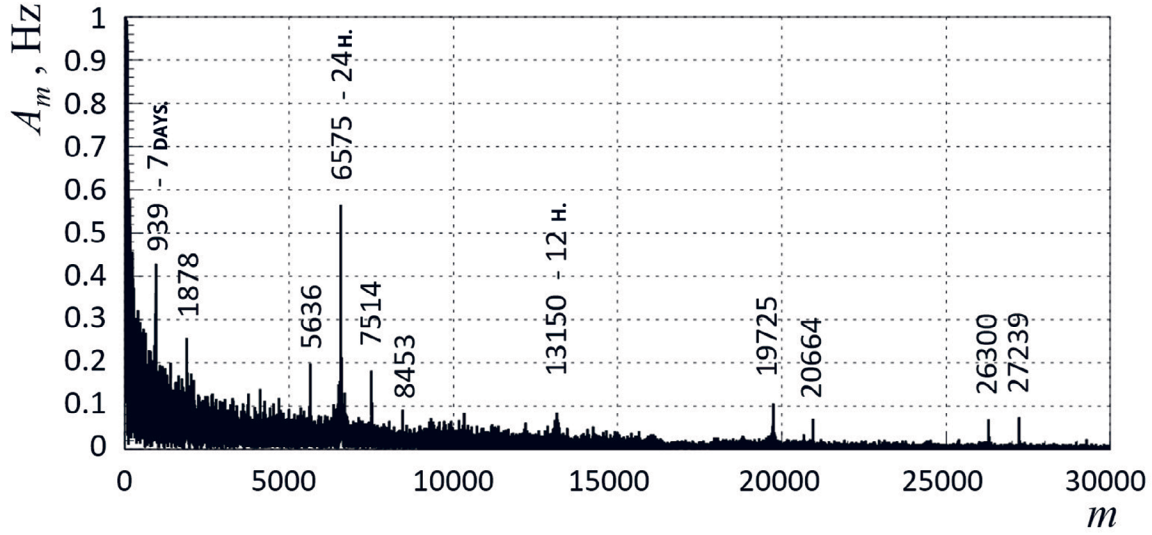

Fig. 1. Fourier harmonics

Table 1. Parameters of main and combination frequencies of visible peaks

Period, days	Frequency f_{comb}	Harmonic number m	A_m, Hz	Visible peak, m	Significance η
7.000	f_2	939	0.43	939	> +10
3.501	$2f_2$	$2 \cdot 939 = 1878$	0.26	1879	+5.98
1.166	$f_1 - f_2$	$6575 - 939 = 5636$	0.20	5635	+4.26
1.000	f_1	6575	0.56	6575	> +10
0.875	$f_1 + f_2$	$6575 + 939 = 7514$	0.18	7515	+3.82
0.778	$f_1 + 2f_2$	$6576 + 2 \cdot 939 = 8453$	0.090	8454	+1.18
0.500	$2f_1$	$2 \cdot 6576 = 13150$	0.077	13149	+0.79
0.333	$3f_1$	$3 \cdot 6576 = 19725$	0.074	19726	+0.70
0.318	$3f_1 + f_2$	$3 \cdot 6575 + 939 = 20664$	0.032	20664	−0.51
0.250	$4f_1$	$4 \cdot 6575 = 26300$	0.038	26301	−0.33
0.241	$4f_1 + f_2$	$4 \cdot 6575 + 939 = 27239$	0.075	27231	+0.74

The value h_m can be negative, meaning the harmonic amplitude is below white noise. The significance of a harmonic shows by how many standard deviations $s(A_m - B)$ the harmonic amplitude exceeds the white noise amplitude.

4. RESULTS OF FOURIER ANALYSIS OF LVD DATA

The result of the Fourier analysis is the amplitudes of harmonics A_m in hertz and their errors, phases of harmonics in radians and their errors, as well as the significance h_m of harmonic amplitudes.

Figure 1 shows the graph obtained using discrete Fourier transform. In some areas of the harmonic spectrum, there are clearly pronounced peaks with highly significant amplitudes — these spectral regions are presented on separate graphs discussed below. On all graphs, the x- axis shows the harmonic numbers.

Let's examine in detail the significant peaks in Figure 1. Let's denote f_1 ($T = 1$ days) the frequency of the most significant harmonic (daily peak) with maximum significant amplitude, and f_2 ($T = 7$ days) — the next harmonic by amplitude. Combination frequencies should mainly depend on these two frequencies: $f_{comb} = (nf_1 \pm kf_2)$, under conditions n, k integers $\geqslant 0$; $f_{comb} > 0$. Table 1 shows eleven harmonic numbers of experimental visible peaks (Fig.1) and their correspondence to harmonic numbers of combination frequencies.

The coincidence of combination frequencies with observed values confirms the correctness of the performed Fourier analysis.

4.1. Solar Diurnal Period (1.00 days = 24h). Wave S1

Let's examine in detail the solar diurnal peak, which has a period of $T = 1$ days = 24h 00 min. This is the diurnal tidal wave S1. Here and further, the wave designations S1, M1, M2, P1, K1 are from the list of main tidal waves according to Melchior [7]. In Fig. 1, this is one of the highest peaks in the area $m = 6575$ with the amplitude of the highest harmonic $A_m = 0.56$ Hz and significance $\mathsf{h}_m > 10$. To the right and left of it, combination frequencies are visible: $(f_1 - f_2)$, harmonic $m = 6575 - 939 = 5636$, significance $\mathsf{h}_m \approx 4.2$, and $(f_1 + f_2)$, harmonic $m = 6575 + 939 = 7514$, significance $\mathsf{h}_m \approx 3.8$. Fig. 2 shows the range of harmonics from $m = 6300$ to $m = 6800$. In the center, a narrow solar diurnal peak several harmonics

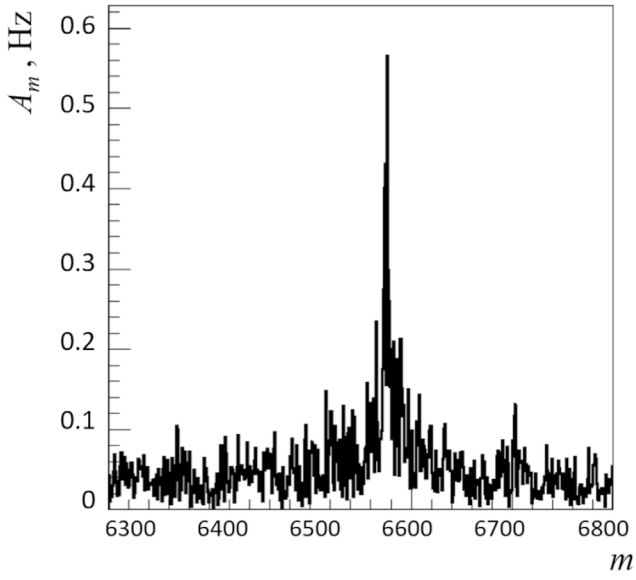

Fig. 2. Fourier harmonics m = 6300 ÷ 6800

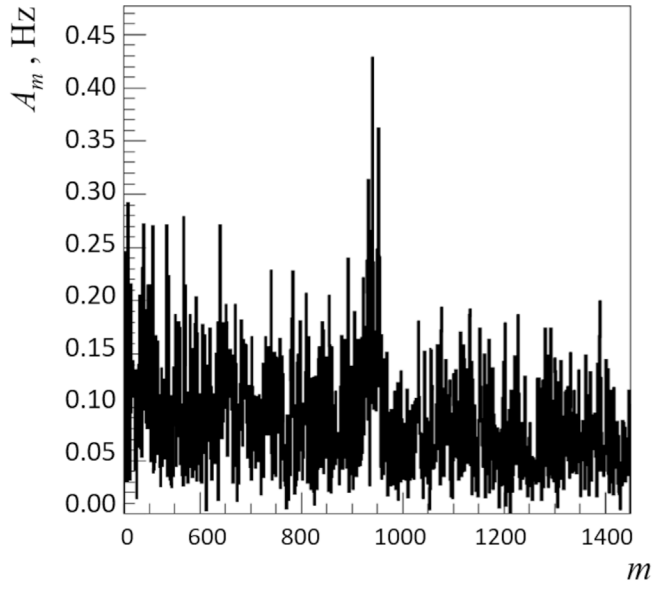

Fig. 3. Fourier harmonics m = 450 ÷ 1450

wide is visible. The peak width at half-height is ~ 5 harmonics.

Solar waves P1 (T = 1.003 days) and K1 (T = 0.997 days) are difficult to distinguish from adjacent nearby peaks.

In the same location T = 1 days, there is a peak from daily human arrivals at the facility and microseismic impact from heavy trucks in transport tunnels. The effect of human technogenic activity on working days was discovered in LVD data in work [5]. Fig. 3 shows harmonics in the range of m = 450∇ · 1450 harmonics. In the center, a "blurred" peak with a period of T = 7 days is visible. The amplitude of the maximum harmonic (m = 940) in the weekly peak is 0.43 Hz, and its significance is $h_m > 10$.

The semidiurnal wave S2 is also visible (harmonic with index m = 13150), but its amplitude is 7 times smaller than the amplitude of wave S1.

4.2 Search for the lunar diurnal period T = (1.01÷1.06) days (wave M1) and semidiurnal period T = (0.505÷0.531) days (wave M2)

Index range m from 6202 to 6509 (width of 307 harmonics) corresponds to T_m = (1.01∇ · 1.06) days — this is the range of the lunar diurnal tidal wave M1. The period of wave M1 is about 24 h 50 min. These are lunar days, which vary throughout the month due to the eccentricity of the Moon's orbit around Earth. The ranges of variation of the S1 and M1 tidal wave periods do not overlap.

Fig. 4 shows harmonics in the range m = 5500÷6600. On the right is the diurnal peak f_1 (m = 6575, T_{6575} = 1 days). On the left is the peak (f_1 - f_2) (m = 6575−939 = 5636) — combination frequency.

Let's take the central part with a width of 154 harmonics (T = 1.0000 days, Fig. 4) here the amplitudes of (m = 6278÷6432) to the left of the solar peak (A_m harmonics should significantly exceed the power-equivalent white noise. Let this be region N4. Let's average all harmonics by power in this region:

$$\bar{A} = \bar{A}_m = \sqrt{\frac{1}{154}\sum_{m=6278}^{6432} A_m^2}.$$

To the left in the spectrum, let's take three more such regions with a width of 154 harmonics each (region numbers N1, N2, N3). To the right of the solar-diurnal peak, let's symmetrically take four more regions (region numbers N5, N6, N7, N8). Thus, the solar-diurnal peak is "cut out" and does not interfere with the search for the lunar peak. Regions (N1-N8) are chosen to avoid combination frequencies (f_1 - f_2) and (f_1 + f_2). We'll take the majority error of one harmonic amplitude $s(A_m)$ as the standard deviation from the mean of harmonic amplitudes across all eight regions: $s(A_m) = 1.61 \times 10^{-2}$ Hz. Let's also calculate the power-equivalent white noise,

Table 2. Parameters of selected regions for finding the lunar-diurnal peak M1

Region	N1	N2	N3	N4	N5	N6	N7	N8
Harmonic range m	5813÷5967	5968÷6122	6123÷6277	6278÷6432	6718÷6872	6873÷7027	7028÷7182	7183÷7337
Period, days,	1.131÷1.102	1.102÷1.074	1.047÷1.047	1.047÷1.022	0.979÷0.957	0.957÷0.936	0.936÷0.915	0.915÷0.896
$\bar{A}\times10^{-2}$, Hz	3.29	3.46	3.52	4.45	3.45	3.13	3.11	2.64
Significance h	−0.96	+0.31	+0.79	+7.96	+0.29	−2.18	−2.37	−5.96

Table 3. Parameters of selected regions for finding the lunar semi-diurnal peak M2

Region	N1	N2	N3	N4
Range m	12373 、 12988	13312 、 13927	13928 、 14543	14544 、 15159
Period, days	0.531 、 0.506	0.494 、 0.472	0.472 、 0.452	0.452 、 0.434
$\bar{A}$, Hz	1.26×10^{-2}	1.114×10^{-2}	1.137×10^{-2}	1.064×10^{-2}
Significance h	+ 5.42	- 1.55	- 0.47	- 3.83

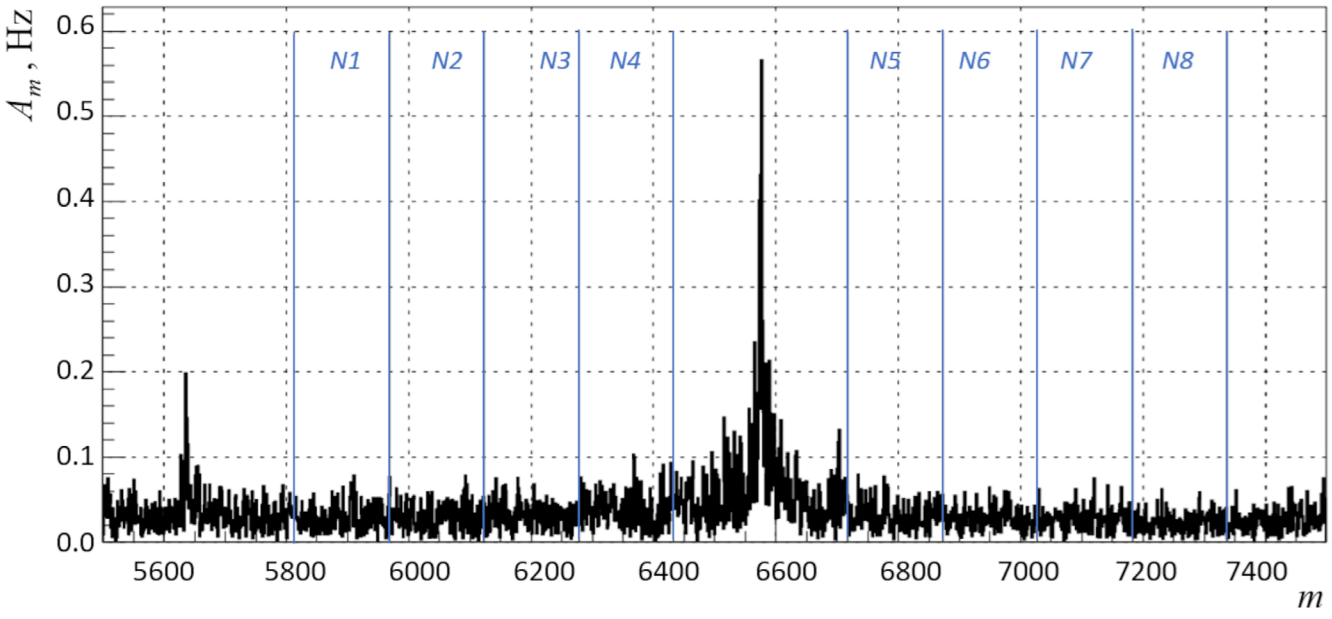

Fig. 4. Fourier harmonics from 5500 to 7600

locally only for the eight regions: $B_m = 3.42 \times 10^2$ Hz $s(B_m) = 4.60 \times 10^{-4}$ Hz for one harmonic).

The calculation results for all N1-N8 regions are presented in Table 2. For each of the regions N1–N8 we obtained $s(\bar{A}) = 1.30 \times 10^{-3}$ Hz, $s(\bar{B}) = 0.37 \times 10^{-4}$ Hz.

We can assert that we see the lunar-diurnal peak $T = (1.01\nabla \cdot 1.06)$days in the expected location for the M1 wave with significance h = 7.96.

Similarly to the M1 wave search, the M2 wave search was conducted (lunar-tidal semi-diurnal wave, its period is 12 h 25.2 min). To the left and right of the S2 wave peak (harmonic index $m = 13150$), regions N1 and N2 with a width of 616 harmonics were selected.

Region N1 is the area of the expected M2 peak location, and region N2 is symmetric relative to S2. Two more regions N3 and N4 are added to the right of N2. Results are summarized in Table 3.

Equivalent power white noise, locally only in four areas: $B_m = 1.148 \cdot 10^{-2}$ Hz, $s(\bar{A} - \bar{B}) = 2.188 \cdot 10^{-4}$ Hz. Wave M2 is visible with significance h = + 5.42.

4.3. Search for synodic lunar-solar period (29.3÷29.8) days

The synodic lunar-solar period is the time interval between two identical phases of the Moon, for example, between two full moons. The gravitational influence of the Moon and Sun creates tidal waves in the Earth with an amplitude on its surface averaging several tens of centimeters.

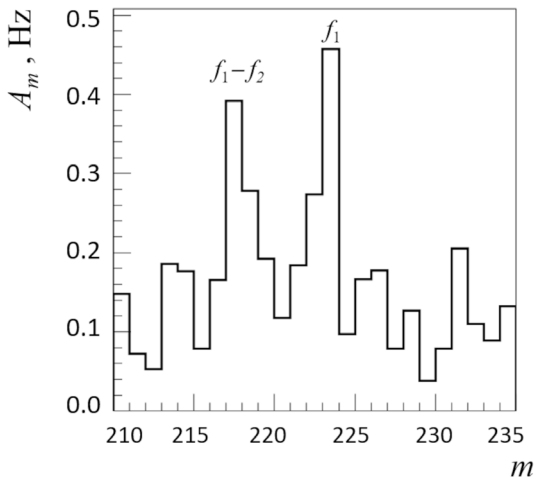

Fig. 5. Fourier harmonics from 210 to 235

The solar-diurnal peak should be around the period of $T_m = 29.5$ days. The area of lunar-solar peak harmonics is shown in Fig. 5. The harmonic with index $m = 223$, with period $T_m = 29.48$ days has significance h = 11.67. The significance decreases sharply to the left and right. But on the left at harmonic $m = 217$ there is a peak with significance h = 9.8, $T_m = 30.30$ days. The peak has the same width as $m = 223$. This is probably a combination frequency.

If f_1 corresponds to $m = 223$ and harmonic for $(f_1 - f_2)$ $m = 217$, then f_2 should correspond to harmonic $m = 6$. Let's see if there is a peak around $m = 6$. In Table 4, there is a clear peak centered at harmonic approximately $m = (5 + 6 + 7 + 8) / 4 = 6.5$. The peak $m = 217$ is likely a combination frequency for three reasons:

a) $A_{217} < A_{223}$;

b) peaks at $m = 217$ and $m = 223$ have the same width, and it equals approximately one harmonic;

c) there is a peak at $m = 6$.

Table 4. Amplitude values for harmonics $m = 4 \div 9$

m	T_m, solar days	A_m, Hz
4	1643	0.92
5	1351	2.45
6	1095	0.31
7	939	1.61
8	822	1.37
9	730	0.32

To more accurately estimate the significance of the lunar-solar peak, we will determine the white noise amplitude B_m using the spectrum section in the area $m = 223$. In Fig. 5, it can be seen that the peak width $T = 29.5$ days can be selected in one harmonic $m = 223$. The amplitude of this harmonic equals $A_{223} = 0.457$ Hz, errors $(A_{223}) = 0.10$ Hz.

The amplitude of each harmonic of the equivalent power white noise (calculated from the vicinity of $m = 210 \div 233$) equals $B_m = 0.19$ Hz, $s(B_m) = 2.05 \times 10^{-2}$ Hz. Under these conditions, the significance of harmonic $m = 223$ equals h = 2.64.

Table 5. Parameters of selected areas for finding the lunar-monthly peak

Area	N1	N2	N3
Harmonics range	224 ÷ 230	231 ÷ 244	245 ÷ 258
Periods, days	29.35 ÷ 28.59	28.46 ÷ 26.94	26.84 ÷ 25.48
Number of harmonics	7	14	14
$\bar{A}$, Hz	0.1187	0.2231	0.1819
Error $s(\bar{A})$, Hz	3.3711^{-2}	2.3838^{-2}	2.3838^{-2}
Error $s(\bar{B})$, Hz	5.6983^{-3}	4.0293^{-3}	4.0293^{-3}
Significance h	−2.074	+1.384	−0.320

Table 6. Parameters of selected areas for finding the annual peak

Area	N1	N2	N3	N4	N5
Range m	9 ÷ 15	16 ÷ 20	21 ÷ 25	26 ÷ 30	31 ÷ 35
Periods, days	730.5 ÷ 438.3	410.9 ÷ 328.7	313.1 ÷ 263.0	252.9 ÷ 219.2	212.1 ÷ 187.9
$\bar{A}$, Hz	0.598	1.168	0.766	0.481	0.424
Significance h	−0.91	+2.59	+0.222	−1.45	−1.79

For the synodic period, where we have one harmonic dominating over the others, we can obtain the phase — the shift of the cosine function maximum relative to the measurement start. Converting the discrete Fourier transform function to cosine, we get $y_m(t) = A_m \cos(\nu_m t + j_m)$, where j_m — phase in radians, ν_m — circular frequency in rad/day ($\nu_m = 2\pi / T_m$), $T_m = 29.5$ days.

We used different sets of statistics from 2004 to 2022. Here we present the most significant results. On six-year statistics from 2004, the phase obtained $j_m = 4.152 \pm 0.083$ rad. Converting radians to days and knowing that the full moon day since 2004 falls on 6.65 days, we calculate the delay of the maximum effect of moon and sun influence on radon emission: $\Delta t = (9.99 - 6.65)$ days $= (3.35 \pm 0.39)$ days.

On ten-year statistics from 2011, the phase obtained is $j_m = 1.49 \pm 0.067$ rad. Converting radians to days and considering the full moon day since2011 (18.89 days), we get a delay of $\Delta t = (22.501 - 18.89)$ days $= (3.61 \pm 0.30)$ days.

Having calculated the average Δt with weight inverse to variances, based on two different statistics, we find that $\Delta t = (3.51 \pm 0.24)$ days after the full moon, LVD "sees" the maximum radon emission through gamma-rays measured by the detector.

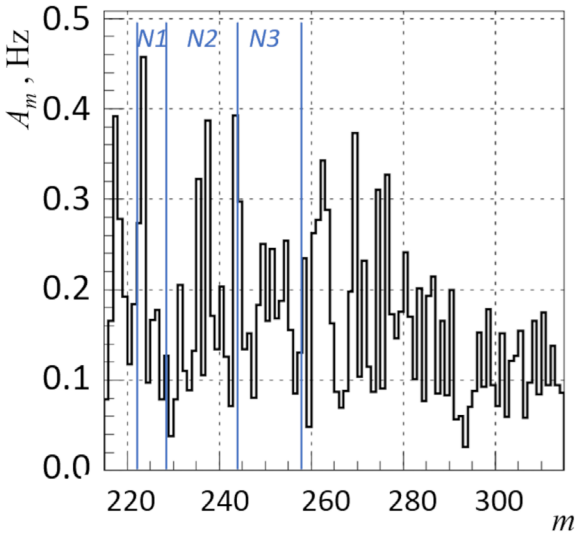

Fig. 6. Fourier harmonics from 215 to 235

4.4. Search for anomalistic lunar-monthly period of 27.55455 days

The Moon, while moving in orbit around planet Earth, passes through the point closest to Earth, the perigee point. The period between two perigees equals $T_a = 27.55455$ days — anomalistic lunar month (Mm wave). Similarly, Earth passes around the Sun over a period of $T = 365.2422$ days between two perihelia — solar year, i.e., returns to the same point in its orbit.

Let's look at the amplitude spectrum of harmonics (Fig. 6) in the range 215 ÷ 315. In the region $m = (226 \div 248) \sim T_m = (29.1 \div 26.5)$ days, harmonics with increased amplitudes are visible — maximum $A_{max} = 0.392$ Гц, $m = 243$. Let's write out harmonics with amplitudes exceeding $A_{max} / 2 = 0.196$ Hz in this area: $m_i = 231, 235, 237, 240, 243, 244$. Let's fix the area of harmonics from 231 to 244 inclusive. We will assume that the majority of the peak power $T_a = 27.5545$ days (width at half-height) is concentrated here. Let's clarify the position of the peak center by averaging all periods T_m within the specified boundaries with a weight equal to the power of harmonics (i.e., squares of amplitudes A_m^2):

$$\bar{T}_m = \frac{\sum_{m=231}^{244} (T_m^2 A_m^2)}{\sum_{m=231}^{244} A_m^2} = 27.54955 \text{ days}.$$

This value coincides with the astronomical period T_a with an accuracy of 0.005 days. Now let's find the significance of the peak: presumably we have a peak in the harmonics region $m = (231 \div 244)$, including 14 harmonics (region N2). Even further left, we cannot take the same region of 14 harmonics $m = (217 \div 230)$ — there is a peak of $T = 29.5$ days. Therefore, we'll take a region of only 7 harmonics $m = (224 \div 230)$ — region N1. And to the right, we can take another region of 14 harmonics $m = (245 \div 230)$ — region N3.

In total, across the three regions N1, N3 we get the white noise amplitude $B_m = 0.190$ Hz. As a result, taking into account the number of harmonics in the regions, we get Table 5. From the calculated parameters $\bar{T}_m = 27.5495$ and significance $\eta = +1.384$ we can only say that there are indications of the existence of a peak in the anomalistic period region.

4.5 Search for the solar-annual period of 365.2422 days

Solar year (or tropical year) is the time interval during which the Sun completes one cycle of seasonal changes as seen from Earth, or the time required for the Sun, starting its motion from a chosen ecliptic longitude, completed one full cycle of seasons and returned to the same ecliptic longitude which is 365 days and 6 hours, more precisely $T = 365.2422$ days.

Figure 7 shows the amplitudes of harmonics in the range $m = 1 \div 35$. Harmonic $m = 18$ corresponds to the period $T_m = 365.27$ days. Let's combine harmonics ($m = 16 \div 20$) around T_m into area N 2. On the left and right, we fix areas N1, N3, N4, N5 (Fig. 7, Table 6). We find the majority root mean square error of one harmonic amplitude $s(A_m) = 0.373$Hz, white noise level $B_m = 0.728$Hz, error $s(B_m) = 7.17 \times 10^{-2}$ Hz and significance η of power-averaged amplitudes by areas. The results are shown in Table 6. The significance of the found peak of the solar annual cycle.

5. DISCUSSION AND CONCLUSION

As a result of Fourier analysis of the time series data from the LVD experiment on the gamma-ray counting rate in the underground, peaks of the following periods were found in the harmonic spectrum with high significance η:

$T = 1$ days, $\eta > 10$ — peak with the highest amplitude, which is contributed to by the effect of solar-diurnal tides in the ground (S1 wave), and

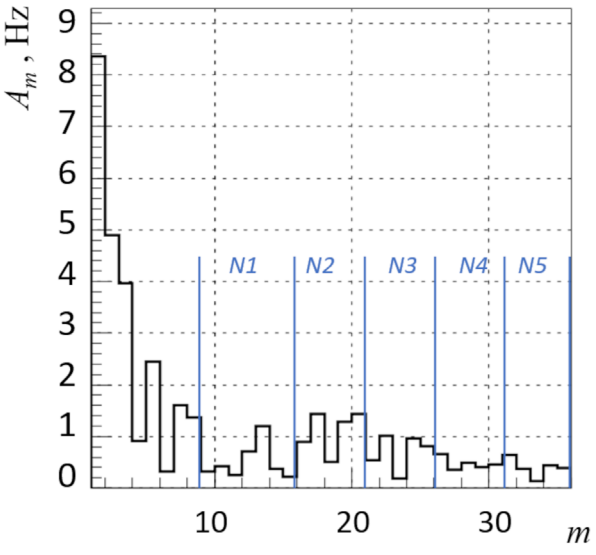

Fig. 7. Fourier harmonics from 1 to 35

is mainly (more than 95%) formed by laboratory personnel activity and truck traffic in transport tunnels;

$T = 7$ days — personnel work in the underground laboratory and automobile traffic in transport tunnels, $h > 10$;

$T = (1.01, 1.06)$ days — period from lunar-diurnal tides in the ground (M1 wave), $h = 8$;

$T = (0.506, 0.531)$ days — period from lunar-semidiurnal tides in the ground (M2 wave),$h = 5.4$. The calculated total power of the M2 peak is less than the total power of the S1 wave peak.

This indicates that the origin of the experimental S1 peak is mainly technogenic and to a lesser extent from the gravitational effects of the Sun.

Periods with low significance:

$T = (29.3, 29.8)$ days — synodic lunar month - period from lunar-solar tides in the ground, $h = 2.7$;

$T = 365.24$ days — annual period between perihelia, $h = 2.6$;

$T = 27.55455$ days — anomalistic lunar month - period between perigees, $h = 1.38$.

In our study, we confirm the presence of gamma-ray variations from natural radioactivity underground related to solar and, to a greater extent, lunar periods, the existence of which was first obtained in the analysis of thermal neutron flux in the surface layer in work [13].

It should be noted that we believe the obtained pink Fourier spectrum (large harmonic amplitudes at low frequencies) is associated with long-term instability of detector counters (mainly photomultipliers), which is corrected by monthly LVD calibrations but is not corrected when measuring the gamma-ray count rate from radon decays in the facility hall. However, this did not prevent finding periods in LVD data related to gravitational effects from the rotation of the Moon and Earth.

The phase — position of the cosine harmonic maximum - was determined for the synodic period($T = 29.5$ days). It was found that$Dt = (3.51 \pm 0.24)$ days after the full moon, LVD "sees" an increase in radon output through gamma rays measured by the detector.

Other phases are difficult to determine since the sought-after periods in the time series of gamma-ray counting rates consist of several harmonics with their own phase. Therefore, the epoch folding method remains the only method for finding the phase for already "known in advance" periods. In the articles using the epoch folding method, phases were found for the annual period (mid-August) and the lunar synodic period (full moon). In work [6], there was an indication of a delay in radon output maximum after the full moon from 1 to 5 days. The obtained result in work [6] confirms the presence of a 3.5-day delay with greater accuracy.

The Earth's crust, like the lithosphere as a whole, under the influence of tidal waves in the Earth is constantly subjected to deformations: during positive half-waves — stretching, and during negative ones — compression. As a result of such deformations in the rocks that make up the Earth's crust, internal stresses arise that affect their physical properties, and the volume of micropores, microcracks, and capillaries changes. Changes in the volumes of micropores, capillaries, and microcracks lead to changes in the ratio of pore and gravitational (free) water volumes in aquifers. Our analysis results confirm that in areas of geophysical faults, the emanation of deep gases increases, correlating with tides in the Earth's crust.

The analysis results will allow to identify (separate) in the experimental data of the detector cases of increased gamma-ray count rate from natural radioactivity associated with gravitational effects, and increases from radon injection during earthquakes in the Italian region.

FUNDING

The study was carried out with financial support from the Russian Science Foundation (grant No. 23-22-00048), https://rscf.ru/project/ 23-22-00048/.

LVD Collaboration: Authors and Affiliations

N. Yu. Agafonova[1], M. Aglietta[2,3], P. Antonioli[4], V. V. Ashikhmin[1], G. Bari[4], G. Bruno[5,6], E. A. Dobrynina[1], R. I. Enikeev[1], W. Fulgione[3,5], P. Galeotti[2,3], M. Garbini[4,7], P. L. Ghia[8], P. Giusti[4], E. Kemp[9], A. S. Malgin[1], A. Molinario[5,10], R. Persiani[4], I. A. Pless[11], O. G. Ryazhskaya[1], G. Sartorelli[4], I. R. Shakiryanova[1], M. Selvi[4], G. C. Trinchero[2,3], C. F. Vigorito[2], V. F. Yakushev[1], and A. Zichichi[4,7]

[1]Institute for Nuclear Research of the Russian Academy of Sciences

117312, Moscow, Russia

[2] Department of Physics, University of Turin and INFN

10125, Turin, Italy

[3] INAF, Osservatorio Astrofisico di Torino

10025, Turin, Italy

[4] University of Bologna and INFN

40127, Bologna, Italy

[5] INFN, Laboratori Nazionali del Gran Sasso

67100, Assergi, L'Aquila, Italy

[6] New York University Abu Dhabi, NYUAD

129188, Abu Dhabi, United Arab Emirates

[7] Centro Enrico Fermi

00184, Roma, Italy

[8] Laboratoire de Physique des 2 Infinis Iréne Joliot Curie, CNRS

91406, Orsay, France

[9] University of Campinas

13083, Campinas, Brazil

[10] Gran Sasso Science Institute

67100, L'Aquila, Italy

[11] Massachusetts Institute of Technology

02139, Cambridge, USA

REFERENCES

1. D. V. Sivukhin, General course of physics, V, Atomic and nuclear physics, Fizmatlit, Moscow (2002)
2. N. Yu. Agafonova, E. A. Dobrynina, N. A. Filimonova, Moscow Univ. Phys. 78, 27 (2023)
3. N.Yu. Agafonova, V.V. Ashikhmin, V.L. Dadykin et al., Bull. Russ. Acad. Sci.: Phys. 81, 512 (2017)
4. N. Y. Agafonova, V. V. Ashikhmin, E. A. Dobrynina, et al., Bull. Russ. Acad. Sci., Physics 83, 614 (2019)
5. N. Yu. Agafonova, E. A. Dobrynina, N. A. Filimonova, et al., JETP 137, 333 (2023)
6. N. Yu. Agafonova, V. V. Ashikhmin, E. A. Dobrynina et al., on behalf of the LVD Collaboration, Phys. Atom. Nuclei 86, 1014 (2023)
7. P. Melchior, Earth's Tides, Mir, Moscow (1968)
8. G. Bari, M. Basile, G. Bruni, et al., Nucl. Instr. Meth. Phys. Res. A 264, 5 (1988)
9. Gran Sasso National Laboratory of the National Institute of Nuclear Physics of Italy https://www.lngs.infn.it (accessed 20.01.2024).
10. G. Bruno, PhD Thesis, Univ. Degli Studi di L'Aquila, L'Aquila (2012).
11. N. Yu. Agafonova, V. A. Alekseev, E. A. Dobrynina, et al., Preprint No. 1071/2001 INR RAS, Moscow (2001)
12. N. Yu. Agafonova, M. Aglietta, P. Antonioli, et al., JETP 134, 449 (2022)
13. V. V. Alekseenko, Y. M. Gavrilyuk, D. D. Dzhappuev, et al., Izvestiya, Phys. Sol. Earth 45, 709 (2009)